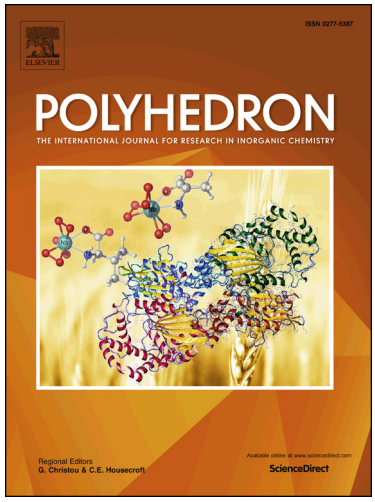

Naphthalenediol-based bis(Salamo)-type homo- and heterotrinuclear cobalt(II) complexes: Syntheses, structures and magnetic properties

Han Zhang, Wen-Kui Dong, Yang Zhang, Sunday Folaranmi Akogun

PII: S0277-5387(17)30407-2
DOI: http://dx.doi.org/10.1016/j.poly.2017.05.051
Reference: POLY 12670

To appear in: *Polyhedron*

Received Date: 2 April 2017
Revised Date: 12 May 2017
Accepted Date: 12 May 2017

Please cite this article as: H. Zhang, W-K. Dong, Y. Zhang, S. Folaranmi Akogun, Naphthalenediol-based bis(Salamo)-type homo- and heterotrinuclear cobalt(II) complexes: Syntheses, structures and magnetic properties, *Polyhedron* (2017), doi: http://dx.doi.org/10.1016/j.poly.2017.05.051

Naphthalenediol-based bis(Salamo)-type homo- and heterotrinuclear cobalt(II) complexes: Syntheses, structures and magnetic properties

Han Zhang, Wen-Kui Dong *, Yang Zhang, Sunday Folaranmi Akogun

School of Chemical and Biological Engineering, Lanzhou Jiaotong University, Lanzhou, Gansu, 730070, P. R. China

ABSTRACT

Homo- and heterotrinuclear Co(II) complexes with a new acyclic bis(Salamo)-type ligand H_4L, which bears a C-shaped O_6 site by the metallation of the N_2O_2 Salamo moieties, were synthesized. The homotrinuclear complex $[Co_3(L)(OAc)_2(CH_3OH)_2]\cdot 2CHCl_3$ (**1**) was obtained by the reaction of H_4L with 3 equivalents of $Co(OAc)_2\cdot 4H_2O$. The heterotrinuclear complexes $[Co_2(L)Ca(OAc)_2]$ (**2**), $[Co_2(L)Sr(OAc)_2]$ (**3**) and $[Co_2(L)Ba(OAc)_2(H_2O)]\cdot 2CH_3CH_2OH$ (**4**) were acquired by the reaction of H_4L with 2 equivalents of $Co(OAc)_2\cdot 4H_2O$ and 1 equivalent of $M(OAc)_2$ (M = Ca(II), Sr(II) and Ba(II)). In the crystal structures, the three metal(II) atoms occupy both the N_2O_2 and O_6 sites of the ligand $(L)^{4-}$ moiety. Owing to the different nature of the N_2O_2 and O_6 sites of the ligand H_4L, the introduction of two different metal(II) atoms to the site-selective moiety, when compared with complex **1**, leads to the replacement of the central Co(II) atom by different alkaline earth metal(II) atoms, namely the Ca(II), Sr(II) and Ba(II) atoms for complexes **2**, **3** and **4**, respectively. Magnetic measurements were performed on complexes **1**-**4**, where an intramolecular ferromagnetic interaction was found in complex **3** and intramolecular antiferromagnetic interactions were found in complexes **1**, **2** and **4**. The magnetic susceptibilities above 50 K obey the Curie-Weiss law and their constant values were determined for all the complexes.

Keywords:

Salamo-type ligand; Trinuclear complex; Synthesis; Crystal structure; Magnetism

* Corresponding authors. Tel: +86 931 4938703; e-mail addresses: dongwk@126.com (W.-K. Dong).

1. Introduction

Salen-type ligands and their corresponding analogues are versatile and important compounds [1-5]. Various kinds of functionalized Salen-type ligands have been synthesized by chemical modification of aldehyde or diamine structures, which can be used for the synthesis of functional metal complexes [6-8]. Salen-type N_2O_2 metal complexes are used as precursors to synthesize oligometallic complexes owing to the high coordination ability of the phenoxo groups which can bridge two metal centers in a μ_2-M–O–M fashion [9-12]. Such μ_2-phenoxo bridging is also particularly important for d-block homo- and heterometallic complexes of Salen-type ligands, some of which exhibit interesting electrochemical [4e,13], fluorescent [2c-2e,4f-4k,7a,7b] and magnetic properties [14a,14b]. According to the recently reported acyclic bis(Salamo)-type ligand H_4L, in which two Salamo chelate moieties share one benzenediol group [15a,15b], when alkoxy groups are introduced at the 3 position of the salicylidene moieties, an O_6 coordination site consisting of the alkoxy groups and phenoxo oxygen atoms is produced in addition to the N_2O_2 site. Thus, the O_6 sites of this type of ligand are particularly suitable for the larger radius of alkaline earth and rare earth metals to afford 3d-2s and 3d-4f heterotrinuclear complexes, which exhibit better magnetic and photochemical properties.

Recently, a part of our research project concentrated on the syntheses of a new acyclic bis(Salamo)-type ligand H_4L, in which two N_2O_2 Salamo chelate moieties share one naphthalenediol group. Due to the presence of O_6 sites in the bis(Salamo)-type ligand H_4L, it was easy to synthesize homo/heterotrinuclear metal complexes [15c-15e]. Here, the central Co(II) atom could be replaced because the six oxygen atoms of the cavity could coordinate to other metal(II) atoms strongly. As a result, taking advantage of the fact that H_4L has both N_2O_2 and O_6 sites with coordinating ability, we have obtained 3d, 3d-2s trinuclear metal complexes and have explored their interesting crystal structures and magnetic properties.

2. Experimental

2.1 Material and general methods

2-Hydroxy-3-methoxybenzaldehyde (99%), methyl trioctyl ammonium chloride (90%), pyridiniumchlorochromate (98%) and borontribromide (99.9%) were purchased from Alfa Aesar.

Hydrobromic acid 33wt% solution in acetic acid was purchased from J&K Scientific Ltd. The other reagents and solvents were purchased from Shanghai Darui Chemical Fine Chemicals Company. Elemental analyses were performed using a GmbH VarioEL V3.00 automatic elemental analysis instrument. FT-IR spectra were recorded on a VERTEX70 FT-IR spectrophotometer, with samples prepared as KBr pellets (400-4000 cm^{-1}). UV-vis absorption spectra were recorded on a Hitachi U-3900H spectrometer. ^{1}H and ^{13}C NMR spectra were determined on a German Bruker AVANCE DRX-400 spectrometer. FTICR-MS spectra were obtained on a Bruker Daltonics APEX-II 47e spectrometer.

2.2 Synthesis of the ligand H_4L

The reaction steps involved in the synthesis of the bis(Salamo)-type tetraoxime ligand (H_4L) are shown in Scheme 1. 2,3-Dihydroxynaphthalene-1,4-dicarbaldehyde was prepared according to a literature procedure [16]; 1,2-bis(aminooxy)ethane and 2-[*O*-(1-ethyloxyamide)]oxime-6-methoxyphenol were synthesized according to an analogous method [14c,14d]. A solution of 2,3-dihydroxynaphthalene-1,4-dicarbaldehyde (432.08 mg, 2 mmol) in ethanol (20 mL) was added dropwise to a solution of 2-[*O*-(1-ethyloxyamide)]oxime-6-methoxyphenol (904.4 mg, 4 mmol) in ethanol (20 mL) at room temperature, the mixture was heated to reflux and kept refluxing for 6 h. After cooling down to room temperature, the obtained yellow precipitates were filtered and washed successively with ethanol and n-hexane. A light yellow powdery solid (H_4L) was obtained and collected by filtration, washed with absolute ethanol and dried under vacuum. Yield: 56.36%; m.p.: 172 ºC; ^{1}H NMR ($CDCl_3$, 400 MHz) δ, ppm: 11.03 (s, 2H), 9.82 (s, 2H), 9.14 (s, 2H), 8.29 (s, 2H), 7.97 (q, J = 3.2 Hz, 2H), 7.41 (q, J = 6.0, 2.9 Hz, 2H), 7.06-6.68 (m, 6H), 4.58 (t, 8H), 3.89 (s, 6H) (Fig. 1). ^{13}C NMR (DMSO, 151 MHz) δ, ppm: 148.43 (s), 148.20 (s), 147.36 (s), 147.22 (s), 146.10 (s), 126.26 (s), 125.40 (s), 123.95 (s), 119.69 (s), 119.04 (s), 118.39 (s), 113.75 (s), 111.42 (s), 73.03 (s), 72.80 (s), 56.31 (s) (Fig. 2). HRMS m/z, Calc. for $C_{32}H_{32}N_4O_{10}Na$: $[H_4L+Na]^+$ 655.20, found: 655.2011 (Fig. 3). Elemental analysis: Anal. Calc. for $C_{32}H_{32}N_4O_{10}$: C, 60.75; H, 5.10; N, 8.86, found (%): C, 60.38; H, 5.38; N, 8.65. IR (KBr; cm^{-1}): 1613 [ν(C=N)], 1254 [ν(Ar-O)], 3167 [ν(O-H)]. UV–vis [in methanol/chloroform (1:1)], λ_{max} (nm) [2.5×10^{-5} M]: 267, 356, 376.

Scheme 1. Synthetic route to the bis(Salamo)-type tetraoxime ligand H_4L.

Fig. 1. ^1H NMR spectrum of the ligand H_4L ($CDCl_3$, 400 MHz).

Fig. 2. ^{13}C NMR spectrum of the ligand H_4L (DMSO, 151 MHz).

Fig. 3. The HRMS of the ligand H_4L.

*2.3 Synthesis of complexes **1**-**4***

Homo- and heterotrinuclear complexes were synthesized by the reaction of H_4L with $M(OAc)_2$ (M(II) = Co(II), Ca(II), Sr(II) and Ba(II)) (Scheme 2). A solution of the ligand H_4L (12.64 mg, 0.020 mmol) in chloroform (4 mL) was added to a solution of $Co(OAc)_2{\cdot}4H_2O$ (14.94 mg, 0.060 mmol) in methanol (4 mL) at room temperature. The color of the solution immediately turned brown. The mixture was filtered and the filtrate was allowed to stand at room temperature for approximately three weeks [14e,15f]. The solvent was partially evaporated and several clear dark brown prismatic single crystals were obtained. Complex **1**, yield: 45.68%. Elemental analysis, Anal. Calc. for $C_{40}H_{44}Cl_6N_4O_{16}Co_3$ (%): C 39.18; H 3.62; N 4.57; Co 14.42. Found (%): C 38.86; H 3.40; N 4.86; Co 14.88. IR (KBr; cm^{-1}): 1606 [ν(C=N)], 1257 [ν(Ar-O)], 3407 [ν(O-H)]. UV-vis [in methanol/chloroform (1:1)], λ_{max}(nm) [2.5×10^{-5} M]: 280, 380, 410.

Scheme 2. Synthesis of the homo- and heterotrinuclear Co(II) complexes.

A solution of $Co(OAc)_2{\cdot}4H_2O$ (9.96 mg, 0.040 mmol) in methanol (2 mL) and $Ca(OAc)_2$ (3.16 mg, 0.020 mmol) in water/methanol (1:3, 2 mL) were added to a solution of H_4L (12.64 mg, 0.020 mmol) in chloroform (4 mL), and the resulting solution was evaporated to dryness, after which the solid was redissolved in chloroform/methanol (1:1, 8 mL). The mixture was filtered and the filtrate was allowed to stand at room temperature for several weeks to obtain complex **2**. Complexes **3** and **4** were prepared by a similar procedure as for complex **2**, however, complex **4** was prepared using ethanol as the solvent instead of methanol that was used for complex **2**.

Complex **2**, dark yellow crystals, yield: 44.65%. Elemental analysis, Anal. Calc. for

$C_{36}H_{34}CaN_4O_{14}Co_2$ (%): C 47.80; H 3.79; N 6.19; Co 13.03; Ca 4.43. Found (%): C 47.49; H 3.23; N 6.42; Co 12.89; Ca 4.20. IR (KBr; cm^{-1}): 1596 [*v*(C=N)], 1250 [*v*(Ar-O)], 3417 [*v*(O-H)]. UV-vis [in methanol/chloroform (1:1)], λ_{max} (nm) [2.5×10^{-5} M]: 290, 373, 415.

Complex **3**, dark orange crystals, yield: 38.69%. Elemental analysis, Anal. Calc. for $C_{36}H_{34}SrN_4O_{14}Co_2$ (%): C 45.41; H 3.60; N 5.88; Co 12.38; Sr 9.20. Found (%): C 45.23; H 3.62; N 5.75; Co 12.26; Sr 8.98. IR (KBr; cm^{-1}): 1596 [*v*(C=N)], 1250 [*v*(Ar-O)], 3417 [*v*(O-H)]. UV-vis [in methanol/chloroform (1:1)], λ_{max} (nm) [2.5×10^{-5} M]: 288, 370, 412.

Complex **4**, dark yellow crystals, yield: 39.65%. Elemental analysis, Anal. Calc. for $C_{39.5}H_{44}BaN_4O_{16.5}Co_2$ (%): C 43.37; H 4.05; N 5.12; Co 10.77; Ba 12.55. Found (%): C 42.98; H 3.72; N 5.52; Co 10.54; Ba 12.31. IR (KBr; cm^{-1}): 1596 [*v*(C=N)], 1250 [*v*(Ar-O)], 3406 [*v*(O-H)]. UV-vis [in methanol/chloroform (1:1)], λ_{max} (nm) [2.5×10^{-5} M]: 282, 389, 420.

2.4 X-ray crystallographic analysis

Single crystals of complexes **1**-**4** were placed on a Bruker Smart 1000 CCD area detector. The diffraction data were collected using graphite monochromated Mo *Kα* radiation (λ = 0.71073 Å) (for **1**, **2** and **4**) and Cu *Kα* radiation (λ = 1.54184 Å) (for **3**). Reflection data were corrected for Lorentz and polarization factors and for absorption using the multi-scan method [17,18]. The structures were solved using the program SHELXL-97 and Fourier difference techniques, and refined by the full-matrix least-squares method on F^2. Anisotropic thermal parameters were used for the non-hydrogen atoms and isotropic parameters for the hydrogen atoms. Hydrogen atoms were added geometrically and refined using a riding model. The crystallographic data are summarized in Table 1.

Table 1 Crystallographic data and refinement parameters for complexes **1**-**4**.

2.5 Cyclic voltammetry

Cyclic voltammetry experiments for complexes **1**–**4** were implemented by an Auto Lab electrochemical workstation (PGSTAT128N, EcoChemie, Netherlands). A conventional three-electrode system was used with a modified glassy carbon (working electrode), Ag/AgCl (reference electrode) and a platinum wire (counter electrode). The sample was made of a 1.0×10^{-3} M DMF solution with the addition of 0.1 M tetrabutylammonium perchlorate (TBAP) as the supporting

electrolyte [19]. The potentials were recorded in the range -1.8 to +1.8 V at a 300 mV/s scan rate.

2.6 Magnetic measurements

Magnetic susceptibility data of the complexes **1**-**4** were collected on powdered samples using a Quantum Design model MPMS XL7 SQUID magnetometer. Magnetic susceptibility measurements were performed at 1000 Oe in the temperature range 2-300 K [2f,20].

3. Results and discussion

The ligand H_4L and its corresponding metal complexes **1**-**4** are stable in air. The ligand H_4L is remarkably soluble in DMF and DMSO, but only slightly soluble in ethyl acetate, acetone, acetonitrile, methanol and ethanol. Complexes **1**-**4** are completely soluble in DMF and DMSO, but only slightly soluble in chloroform, methanol and ethanol at room temperature.

3.1 IR spectra analyses

The IR spectra of H_4L and its corresponding Co(II) complexes **1**-**4** exhibit various bands in the region of 4000-400 cm^{-1} (Fig. 4). The spectrum of the ligand shows an O–H stretching band at 3167 cm^{-1} that belongs to the phenolic hydroxyl group, whereas complex **1** shows a band at 3407 cm^{-1} that belongs to coordinated methanol molecules. The free ligand H_4L exhibits characteristic C=N and Ar–O stretching bands at 1613 and 1254 cm^{-1}, respectively, which are shifted by *ca*. 8 and 5 cm^{-1} in complex **1**. This lowering of energy results from the Co–N and Co–O interactions upon complexation, which is similar to previously reported Co(II) complexes [10b]. Compared with complex **1**, the C=N and Ar–O stretching bands belonging to the heterotrinuclear complexes are shifted by *ca*. 4~7 and 6~8 cm^{-1}, respectively. This results from replacing the central Co(II) atom by the M(II) atom and forming new M–O and M–N coordination bonds. Meanwhile, the O–H stretching band disappeared for complexes **2** and **3**. The O–H stretching band at 3417 cm^{-1} belonging to a water molecule of complex **4** is shifted by *ca.* 10 cm^{-1}. The above facts are consistent with the results determined by X-ray diffraction.

Fig. 4. IR spectra of the ligand H_4L and its corresponding complexes **1**-**4**.

3.2 UV-vis spectral analyses

Methanol/chloroform (1:1) solutions of the ligand H_4L and its homo/heterotrinuclear Co(II) complexes show, as expected, almost identical UV-vis spectra (Fig. 5). The free ligand H_4L shows three strong absorption bands at 267, 356 and 376 nm. The absorption peak at 267 nm can be assigned to the π–π^* transition of the benzene rings and the other two bands at 356 and 376 nm can be attributed to the intra-ligand π-π* transition of the C=N bonds [4i]. Compared to the absorption peaks of the free ligand H_4L, corresponding absorption peaks at *ca*. 380 and 410 nm are observed in complexes **1**-**4**, which are bathochromically shifted, indicating the coordination of the metal(II) atoms with the free ligand H_4L. The auxochromes (–OH) attached to the benzene and naphthalene rings could be responsible for the bathochromic shift observed in the absorption peaks [14f,6b,14g]. In summary, it is evident that complexes **1**-**4** containing benzene and naphthalene rings were synthesized.

Fig. 5. UV-vis spectra of the ligand H_4L and its corresponding complexes **1**-**4** in methanol/chloroform (1:1) ($c = 2.5 \times 10^{-5}$ M).

3.3 HRMS analyses

The synthesized Co(II) complexes **1**-**4** were further characterized by high resolution mass spectrometry (HRMS). The HRMS of complex **1** was consistent with the proposed empirical formula (Fig. 6), with m/z = 804.9855 $[M\text{-}2CH_3COO\text{-}2CH_3OH]^{2+}$, calcd = 804.98. The HRMS of complexes **2** and **3** were also consistent with the proposed empirical formulae (Fig. 7, Fig. 8), with m/z = 786.0127 $[M\text{-}2CH_3COO]^{2+}$, calcd = 786.01 and m/z = 833.9557 $[M\text{-}2CH_3COO]^{2+}$, calcd = 833.95. The HRMS of complex **4** was consistent with the proposed empirical formula (Fig. 9), with m/z = 901.0833 $[M\text{-}2CH_3COO\text{-}2CH_3CH_2OH]^{2+}$, calcd = 901.96. Therefore, the discrete trinuclear structures of the complexes in solution were confirmed by HRMS.

Fig. 6. The HRMS of complex **1**.

Fig. 7. The HRMS of complex **2**.

Fig. 8. The HRMS of complex **3**.

Fig. 9. The HRMS of complex **4**.

3.4 Description of the crystal structures

The structures of the homo- and heterotrinuclear complexes were determined by single-crystal X-ray diffraction. Selected bond lengths and angles of complexes **1**-**4** are listed in Table 2.

Table 2 Selected bond lengths (Å) and angles (°) of complexes **1**-**4**.

*3.4.1 Crystal structure of complex **1***

The crystal structure and atom numbering of complex **1** is shown in Fig. 10. Complex **1** crystallizes in the monoclinic crystal system, space group $P2_1/n$. X-ray crystallography clearly shows the formation of complex **1**, which was isolated as dark brown crystals. Interestingly, the formation process of complex **1** was highly cooperative. In the crystal structure of complex **1**, two terminal Co(II) atoms (Co1 and Co2) are located in the N_2O_2 cavities of the Salamo moieties, while the third one (Co3) is located in the central O_6 cavity. Two chelating acetate ions bridge the trinuclear Co(II) atoms in a familiar μ_2-fashion, which probably contributes to the cooperative formation of complex **1**. The terminal Co(II) atoms (Co1 and Co2) are both penta-coordinated with distorted trigonal bipyramidal geometries, which were deduced by calculating the value of $\tau_1 = 0.7268$ and $\tau_2 = 0.8743$, respectively [21]. The distances between the Co3 atom and the coordinated oxygen atoms range from 2.027(3) to 2.150(4) Å. The central Co3 atom is hexa-coordinated in the central O_6 cavity and has a distorted octahedral geometry with six oxygen-donor atoms, including two μ_2-acetato ligands, phenoxy oxygen groups and methanol molecules.

Fig. 10. (a) View of the molecular structure of complex **1** (hydrogen atoms and solvent molecules are omitted for clarity and thermal ellipsoids are drawn at the 30% probability level). (b) Coordination polyhedra for the Co(II) atoms of complex **1**.

As a result, when the two N_2O_2 Salamo moieties are metallated with d-block transition metals,

the conformation of the molecules is restricted so that the phenoxo oxygen atoms are directed inward to form an O_6 cavity. The complexation of the $(L)^{4-}$ unit with the Co(II) atom takes place in a cooperative fashion and produces the homotrinuclear complex $[Co_3(L)]^{2+}$, in which the third Co(II) atom is in the O_6 cavity. However, the size of the O_6 cavity seems to be too large to fit the central Co(II) atom because only two oxygen donor atoms coordinate to the central Co(II) atom in the crystal structure. Thus, this structure suggests that the central Co(II) atom could be replaced by another metal(II) atomswith a suitable size for the O_6 cavity, such as Ca(II), Sr(II) or Ba(II), to form a C-shaped complex.

3.4.2 Crystal structure of complex ***2***

The crystal structure and atom numbering of complex **2** is shown in Fig. 11. Complex **2** crystallizes in the triclinic crystal system, space group $\bar{P}1$. In complex **2**, two terminal Co(II) atoms (Co1 and Co2) are located in the N_2O_2 sites of the Salamo moieties, two chelating acetate ions bridge the Co(II) atoms and the Ca(II) atom in a μ_2-fashion. The Co1 and Co2 atoms are both penta-coordinated with distorted tetragonal pyramidal geometries, which were deduced by calculating the value of τ_3 = 0.3828 and τ_4 = 0.0453, respectively [21]. The central Ca1 atom is octa-coordinated with a distorted square antiprism geometry, replacing the central Co(II) atom of complex **1**. Here, all the six oxygen atoms of the $[Co_2(L)]$ moiety coordinate nicely to the Ca(II) atom. Complex **2** has strong coordination with methoxy groups, determined by analyzing the distances between the Ca1 atom and the oxygen atoms of the methoxy groups. The distances between the Ca1 atom and the four phenoxy oxygen atoms of the Salamo moieties range from 2.384(3) to 2.435(3) Å, which are obviously shorter than the methoxy groups (Ca1–O1 2.604(3) Å and Ca1–O10 2.612(3) Å). This fact clearly shows this C-shaped O_6 cavity is suitable for more metal(II) atoms of different sizes and it is easy to form heterotrinuclear complexes.

Fig. 11. (a) View of the molecular structure of complex **2** (hydrogen atoms are omitted for clarity, and thermal ellipsoids are drawn at the 30% probability level). (b) Coordination polyhedra for the Co(II) and Ca(II) atoms of complex **2**.

As a result, the stable complex **2** was synthesized by the reaction of H_4L with 2 equivalents of

$Co(OAc)_2 \cdot 4H_2O$ and 1 equivalent of $Ca(OAc)_2$, in which the Ca(II) atom is in the O_6 cavity. Compared with complex **1**, the Ca(II) atom has stronger coordination with the oxygen atoms of the methoxy groups, which probably results from its larger radius compared to the Co(II) atom.

*3.4.3 Crystal structure of complex **3***

The crystal structure and atom numbering of complex **3** is depicted in Fig. 12. Complex **3** crystallizes in the triclinic crystal system, space group $\overline{P}1$. The Co(II) atoms of complex **3** have similar coordination environments and geometries, with τ values of τ_5 = 0.4508 (Co1) and τ_6 = 0.1733 (Co2) [21]. They are both penta-coordinated with distorted tetragonal pyramidal geometries. The central Sr1 atom is octa-coordinated with a distorted hexagonal bipyramidal geometry, which is different from the Ca1 atom of **2**. The distances between the Sr1 atom and the four phenoxy oxygen atoms of the Salamo moieties range from 2.521(4) to 2.565(5) Å, which are clearly shorter than those to the methoxy groups (Sr1–O1 2.650(4) Å and Sr1–O10 2.672(4) Å). Obviously, the Sr–O bond lengths in complex **3** are larger than the corresponding Ca–O bond lengths found in complex **2**.

Fig. 12. (a) View of the molecular structure of complex **3** (hydrogen atoms are omitted for clarity, and thermal ellipsoids are drawn at the 30% probability level). (b) Coordination polyhedra for the Co(II) and Sr(II) atoms of complex **3**.

*3.4.4 Crystal structure of complex **4***

The crystal structure and atom numbering of complex **4** is shown in Fig. 13. Complex **4** crystallizes in the triclinic crystal system, space group $\overline{P}1$, which is similar to complexes **2** and **3**. The Co(II) atoms of complex **4** are both penta-coordinated with tetragonal pyramidal and trigonal bipyramidal geometries for the Co1 and Co2 atoms, respectively, which were obtained by calculating the τ values, τ_7 = 0.38 and τ_8 = 0.7383 for Co1 and Co2, respectively [21]. Owing to the coordination of one water molecule, the central Ba1 atom is nona-coordinated with a distorted tricapped trigonal prismatic geometry, which is different from the Ca1 and Sr1 atoms of complexes **2** and **3**. The distances between the Ba1 atom and the four phenoxy oxygen atoms of the Salamo moieties range from 2.733(5) to 2.851(5) Å, which are evidently shorter than the distances to the methoxy groups (Ba1–O1 2.975(5) Å and Ba1–O10 3.109(5) Å). The same situation was observed in complexes **2**

and **3**.

Fig. 13. (a) View of the molecular structure of complex **4** (hydrogen atoms and solvent molecules are omitted for clarity, and thermal ellipsoids are drawn at the 30% probability level). (b) Coordination polyhedra for the Co(II) and Ba(II) atoms of complex **4**.

Therefore, the resulting geometries of the Co1 and Co2 atoms are both penta-coordinated square pyramidal and the Ca1 and Sr1 are both octa-coordinated with square antiprismatic and distorted hexagonal bipyramidal geometries, respectively. However, the Ba1 atom is larger than the size of the cavity, so coordination of the Ba1 atom with a water molecule makes the structure more stable. The resulting geometry of the Ba1 atom is the rare single square tricapped trigonal prism. As the cation radius increases, the coordination bond lengths of the central cation are distinctly becoming larger and larger. This fact suggests that the radius size of central cation is a significant factor which affects the binding ability of the central O_6 site. As a result, the coordinating capability in the central O_6 site is in the order Ca(II) > Sr(II) > Ba(II).

3.5 Cyclic voltammetry

The electrochemistry of the four complexes **1**-**4** was studied by cyclic voltammetry using DMF as the solvent. Fig. 14 shows the cyclic voltammograms for complexes **1**-**4** in the potential range -1.8 to 1.8 V. The plot for complex **1** exhibits two different redox pairs. The first anodic/cathodic couple potential (E_{pa} = -0.758, E_{pc} = -0.670) is attributed to the Co(II)(Salamo)/Co(I)(Salamo) process (Co(II)(Salamo) + e ↔ Co(I)(Salamo)). The ratio of the anodic to cathodic peak currents I_{pa}/I_{pc} = 2.201 (I_{pa} = -22.09, I_{pc} = 10.04) and $\Delta E = |E_{pa} - E_{pc}|$ = 0.088 V are in agreement with a quasi-reversible electron-transfer process [4e,22]. The second couple potential is attributed to the Co(II/I)(Salamo) process, but an anodic peak is not observed, indicating an irreversible redox process. The cathodic peak potential is observed at E_{pc} = 1.042 V which corresponds to the Co(III)(Salamo) + e ↔ Co(II)(Salamo) process. In this system, the Co(II)(Salamo) complex is more stable than the Co(III)(Salamo) complex. A similar argument is applicable to the remaining Co(II) complexes (**2**-**4**).

Fig. 14. Cyclic voltammograms of 10^{-3} M solutions of **1**-**4** in DMF. Rate = 300 mv/s.

3.6 Magnetic properties

Powder X-ray diffraction (PXRD) data were recorded by a RIGAKU-DMAX2500 X-ray diffractometer using Cu *Kα* radiation (λ = 0.154 nm) at a scanning rate of 5°/min for 2θ ranging from 5° to 50°. (Fig. 15) The PXRD data at room temperature on the samples of complexes **1**-**4** well matched the calculated results from single crystal data. We determined the magnetic susceptibility of crystal samples of the four complexes in the temperature range 2.0-300 K. The temperature dependence of the magnetic susceptibilities complex **1** is shown in Fig. 16, as a plot of $\chi_M T$ versus T. The $\chi_M T$ value for the homotrinuclear complex **1** is 9.42 cm^3 K mol^{-1} at 300 K, which is higher than the calculated value of 5.625 cm^3 K mol^{-1} expected for three high spin Co(II) ($3d^7$, S = 3/2) non-interacting ions [23-26]. On lowering the temperature, the $\chi_M T$ value kept decreasing smoothly and reached a value of 8.32 cm^3 K mol^{-1} at *ca*. 50 K, followed by a rapid decrease. The $\chi_M T$ value decreased with decreasing temperature, indicating an intramolecular antiferromagnetic interaction between the three Co(II) atoms. At 2 K, the $\chi_M T$ value reached a minimum value of 5.36 cm^3 K mol^{-1}. The reciprocal susceptibility ($1/\chi_M$) of complex **1** obeys the Curie-Weiss law with θ = -5.5723 K and C = 9.335 cm^3 K mol^{-1} (Fig. 16, inset) [27-32]. A negative Weiss constant again confirms the antiferromagnetic interaction exhibited by complex **1**.

Fig. 15. PXRD patterns for the homo- and heterotrinuclear complexes **1**-**4**.

Fig. 16. Plot of $\chi_M T$ vs. T for complex **1** between 2 and 300 K. Inset: Temperature dependence of χ_M^{-1}. The red solid line represents the best fitting results.

The temperature dependence of the magnetic susceptibilities of complex **2** is shown in Fig. 17, as a plot of $\chi_M T$ against T. The $\chi_M T$ value of 4.97 cm^3 K mol^{-1} at 300 K for the heterotrinuclear complex **2** is slightly higher than the value of 4.73 cm^3 K mol^{-1} expected for two Co(II) ($3d^7$, S=3/2) and one Ca(II) (S=0) magnetically isolated ions. Because the Ca(II) ions have no single unpaired electrons, they exhibit weak paramagnetism and can be neglected [33,34]. Upon cooling, the $\chi_M T$

value decreased gradually to reach a value of 4.68 cm^3 K mol^{-1} at *ca*. 50 K and then rapidly decreased to reach a value of 3.01 cm^3 K mol^{-1} at 2 K. Therefore, the magnetic susceptibilities ($1/\chi_M$) obey the Curie–Weiss law in the temperature range 2-300 K for complex **2**, giving a positive Weiss constant θ = -3.7864 K and C = 4.921 cm^3 K mol^{-1} (Fig. 17, inset), again confirming the antiferromagnetic interaction exhibited by complex **2**, which is consistent with complex **1**.

Fig. 17. Plot of $\chi_M T$ vs. T for complex **2** between 2 and 300 K. Inset: Temperature dependence of χ_M^{-1}. The red solid line represents the best fitting results.

The temperature dependence of the magnetic susceptibilities of complex **3** is shown in Fig. 18, depicting a plot of $\chi_M T$ against T. The plots for complex **3** display different magnetic characteristics when compared with complexes **1** and **2**. The $\chi_M T$ value of 5.54 cm^3 K mol^{-1} at 300 K for complex **3** is slightly higher than the value of 4.73 cm^3 K mol^{-1} expected for two Co(II) ($3d^7$, S=3/2) and one Sr(II) (S=0) magnetically isolated ions [35,36]. On lowering the temperature to 35 K, the $\chi_M T$ value decreased slowly, and when the temperature was further decreased, the $\chi_M T$ value increased sharply and reached a maximum value of 8.07 cm^3 K mol^{-1} at 12 K. Finally, a further decrease in temperature, resulted in a sharp decline in $\chi_M T$, reaching a value of 4.32 cm^3 K mol^{-1} at 2 K. The trend of the change in $\chi_M T$ values with temperature in the region above 12 K could be an indicator that the two Co(II) atoms in complex **3** are ferrimagnetically interacting. In addition, when the temperature dropped below 12 K, the sharp decrease in the $\chi_M T$ value is mainly due to the interaction between antiferromagnetic molecules, Zero-field splitting and Zeeman effects. The magnetic susceptibilities ($1/\chi_M$) obey the Curie-Weiss law in the temperature range 2-300 K for complex **3**, giving a positive Weiss constant θ = -0.3245 K and C = 5.294 cm^3 K mol^{-1} (Fig. 18, inset), again confirming the antiferromagnetic interaction exhibited by complex **3**.

Fig. 18. Plot of $\chi_M T$ vs. T for complex **3** between 2 and 300 K. Inset: Temperature dependence of χ_M^{-1}. The red solid line represents the best fitting results.

The temperature dependence of the magnetic susceptibilities of complex **4** is given in Fig. 19, as a plot of $\chi_M T$ versus T. The $\chi_M T$ value at 300 K for complex **4** is 9.45 cm^3 K mol^{-1}, which is higher

than the calculated value of 4.73 cm^3 K mol^{-1} expected for two Co(II) ($3d^7$, S=3/2) magnetically isolated ions. However, the value of $\chi_M T$, which is different from that of complex **2**, gradually increased with decreasing temperature, and reached a maximum value of 10.44 cm^3 K mol^{-1} at 70 K; finally, the $\chi_M T$ value reduced to 8.10 cm^3 K·mol^{-1} when the temperature reached 2 K. The trend of the change in $\chi_M T$ value with temperature in the region above 70 K could a proof that the two Co(II) atoms in complex **4** are ferromagnetically interacting. The magnetic susceptibilities ($1/\chi_M$) obey the Curie–Weiss law in the temperature range 2-300 K for complex **4**, giving a positive Weiss constant θ = 1.4257 K and C = 9.653 cm^3 K mol^{-1} (Fig. 19, inset), confirming the ferromagnetic interaction exhibited by complex **4**. The complexes have the same ligand but different coordination environments, so their magnetic behaviors are different. The results show that the coordination environment of the metal ions has some influence on the magnetic properties.

Fig. 19. Plot of $\chi_M T$ vs. T for complex **4** between 2 and 300 K. Inset: Temperature dependence of χ_M^{-1}. The red solid line represents the best fitting results.

4. Conclusion

The homo- and heterotrinuclear Co(II) complexes **1**-**4** have been designed and synthesized. Their X-ray crystal structures reveal that the different nature of the N_2O_2 and O_6 sites of the ligand H_4L leads to the site-selective introduction of two different kinds of metal(II) atoms for the replacement of the central Co(II) atom by Ca(II), Sr(II) and Ba(II) atoms. The coordination number of the Co(II), Ca(II), Sr(II) and Ba(II) atoms in the O_6 environment are 6, 8, 8 and 9, respectively, and have slightly distorted octahedral, square antiprismatic, hexagonal bipyramidal and square tricapped trigonal prismatic geometries. As a result, the coordinating capability in the central O_6 site is in the order Ca(II) > Sr(II) > Ba(II). The magnetic properties of all these complexes were studied. For complex **1**, the $\chi_M T$ value was directly proportional to temperature change, thereby, showing an antiferromagnetic interaction between the three Co(II) atoms. In contrast, the $\chi_M T$ values of complexes **2**-**4** showed anomalous behavior to a change in temperature, with different magnetic coupling effects. The measurement of cyclic voltammetry potentials and magnetic properties of the complexes indicated the complexes could show a good application for molecular materials. Owing to

their electrostatic interaction and their size-fit principle, rare-earth(III) atoms should replace the central Co(II) atom successfully, which could be used for the recognition of rare-earth(III) atoms and for the study of the magnetic properties of 3d-4f complexes. Related research is underway.

Acknowledgements

This work was supported by the National Natural Science Foundation of China (21361015), which is gratefully acknowledged.

Appendix A. Supplementary data

CCDC 1519396, 1519397, 1519394 and 1519395 contain the supplementary crystallographic data for **1**, **2**, **3** and **4**. These data can be obtained free of charge via http://www.ccdc.cam.ac.uk/conts/retrieving.html, or from the Cambridge Crystallographic Data Centre, 12 Union Road, Cambridge CB2 1EZ, UK; fax: (+44) 1223-336-033; or e-mail: deposit@ccdc.cam.ac.uk.

References

[1] (a) H.L. Wu, G.L. Pan, Y.C. Bai, H. Wang, J. Kong, F.R. Shi, Y.H. Zhang, X.L. Wang, J. Chem. Res. 38 (2014) 211; (b) H.L. Wu, G.L. Pan, Y.C. Bai, H. Wang, J. Kong, F.R. Shi, Y.H. Zhang, X.L. Wang, Res. Chem. Intermed. 41 (2015) 3375; (c) H.L. Wu, Y.C. Bai, Y.H. Zhang, Z. Li, M.C. Wu, C.Y. Chen, J.W. Zhang, J. Coord. Chem. 67 (2014) 3054; (d) H.L. Wu, C.P. Wang, F. Wang, H.P. Peng, H. Zhang, Y.C. Bai, J. Chinese Chem. Soc. (2015) 1028; (e) C.Y. Chen, J.W. Zhang, Y.H. Zhang, Z.H. Yang, H.L. Wu, G.L. Pan, Y.C. Bai, J. Coord. Chem. 68 (2015) 1054; (f) H.L. Wu, Y.C. Bai, Y.H. Zhang, G.L. Pan, J. Kong, F.R. Shi, X.L. Wang, Z. Anorg, Allg. Chem. 640 (2014) 2062; (g) H.L. Wu, G.L. Pan, Y.C. Bai, Y.H. Zhang, H. Wang, F.R. Shi, X.L. Wang, J. Kong, J. Photochem. Photobio. B 135 (2014) 33; (h) H.L. Wu, G.L. Pan, Y.C. Bai, H. Wang, J. Kong, F.R. Shi, Y.H. Zhang, X.L. Wang, J. Coord. Chem. 66 (2013) 2634.

[2] (a) X.Q. Song, P.P. Liu, Z.R. Xiao, L. Xia, Y.A. Liu, Inorg. Chim. Acta 438 (2015) 232; (b) P.P. Liu, W.S. Liu, X.Q. Song, W.Y. Xu, Y.A. Liu, Inorg. Chim. Acta 434 (2015) 252; (c) X.Q. Song, Y.J. Peng, G.Q. Chen, X.R. Wang, P.P. Liu, W.Y. Xu, Inorg. Chim. Acta 427 (2015) 13; (d) X.Q. Song, L. Wang, Q.F. Zheng, W.S. Liu, Inorg. Chim. Acta 391 (2012) 171; (e) X.Q. Song, G.Q. Cheng, X.R. Wang, W.Y. Xu, P.P. Liu, Inorg. Chim.

Acta 425 (2015) 145; (f) X.Q. Song, P.P. Liu, Y.A. Liu, J.J. Zhou, X.L. Wang, Dalton Trans. 45 (2016) 8154.

[3] (a) Y.X. Sun, X.H. Gao, Synth. React. Inorg. Met.-Org. Nano-Met. Chem. 41 (2011) 973; (b) Y.X. Sun, L. Wang, X.Y. Dong, Z.L. Ren, W.S. Meng, Synth. React. Inorg. Met.-Org. Nano-Met. Chem. 43 (2013) 599; (c) Y.X. Sun, W.K. Dong, L. Wang, L. Zhao, Y.H. Yang, Chinese J. Inorg. Chem. 25 (2009) 1478; (d) Y.X. Sun, S.T. Zhang, Z.L. Ren, X.Y. Dong, L. Wang, Synth. React. Inorg. Met. Org. Nano Met. Chem. 43 (2013) 995; (e) Y.X. Sun, L. Xu, T.H. Zhao, S.H. Liu, G.H. Liu, X.T. Dong, Synth. React. Inorg. Met. Org. Nano Met. Chem. 43 (2013) 509.

[4] (a) W.K. Dong, X.L. Li, L.Y. Zhang, Y.J. Dong, Sens. Actuators, B 229 (2016) 370; (b) W.K. Dong, P.F. Lan, W.M. Zhou, Y. Zhang, J. Coord. Chem. 69 (2016) 1272; (c) W.K. Dong, L.C. Zhu, J.C. Ma, Y.X. Sun, Y. Zhang, Inorg. Chim. Acta 453 (2016) 402; (d) W.K. Dong, S.F. Akogun, Y. Zhang, Y.X. Sun, X.Y. Dong, Sens. Actuators, B 238 (2017) 723; (e) W.K. Dong, J.C. Ma, L.C. Zhu, Y. Zhang, X.L. Li, Inorg. Chim. Acta 445 (2016) 140; (f) B.J. Wang, W.K. Dong, Y. Zhang, S.F. Akogun, Sens. Actuators, B DOI: 10.1016/j.snb.2017.02.154, 2017, In press; (g) J.C. Ma, X.Y. Dong, W.K. Dong, Y. Zhang, L.C. Zhu, J.T. Zhang, J. Coord. Chem. 69 (2016) 149; (h) Y.J. Dong, J.C. Ma, L.C. Zhu, W.K. Dong, Y. Zhang, J. Coord. Chem. 70 (2017) 103; (i) W.K. Dong, L.C. Zhu, Y.J. Dong, J.C. Ma, Y. Zhang, Polyhedron 117 (2016) 148; (j) Y.J. Dong, X.Y. Dong, W.K. Dong, Y. Zhang, L.S. Zhang, Polyhedron 123 (2017) 305; (k) W.K. Dong, F. Zhang, N. Li, L. Xu, Y. Zhang, J. Zhang, L.C. Zhu, Z. Anorg, Allg. Chem. 642 (2016) 532.

[5] (a) X.J. Li, F.L. Jiang, L. Chen, M.Y. Wu, S. Lu, J.D. Pang, K. Zhou, X.Y. Chen, M.C. Hong, Cryst Eng Comm. 18 (2016) 2239; (b) G.W. Gokel, W.M. Leevy, M.E. Weber, Chem. Rev. 104 (2004) 2723.

[6] (a) P. Wang, L. Zhao, Spectrochim. Acta, Part A 135 (2015) 342; (b) P. Wang, L. Zhao, Synth. React. Inorg. Met.-Org. Nano-Met. Chem. 46 (2016) 1095; (c) X.Y. Dong, Y.X. Sun, L. Wang, L. Li, J. Chem. Res. 36 (2012) 387; (d) L. Zhao, L. Wang, Y.X. Sun, W.K. Dong, X.L. Tang, X.H. Gao, Synth. React. Inorg. Met. Org. Nano Met. Chem. 42 (2012) 1303; (e) L. Zhao, X.T. Dang, Q. Chen, J.X. Zhao, L. Wang, Synth. React. Inorg. Met. Org. Nano Met. Chem. 43 (2013) 1241.

[7] (a) T.Z. Yu, K. Zhang, Y.L. Zhao, C.H. Yang, H. Zhang, L. Qian, D.W. Fan, W.K. Dong, L.L. Chen, Y.Q. Qiu, Inorg. Chim. Acta 361 (2008) 233; (b) T.Z. Yu, K. Zhang, Y.L. Zhao, C.H. Yang, H. Zhang, D.W. Fan, W.K. Dong, Inorg. Chem. Commun. 10 (2007) 401; (c) T.Z. Yu, W.M. Su, W.L. Li, Z.R. Hong, R.N. Hua, M.T. Li, B. Chu, B. Li, Z.Q. Zhang, Z. Hu, Inorg. Chim. Acta 359 (2006) 2246.

[8] (a) L. Xu, Y.P. Zhang, J.Y. Shi, W.K. Dong, Chinese J. Inorg. Chem. 23 (2007) 1999; (b) L. Xu, Y.P. Zhang, L. Wang, J.Y. Shi, W.K. Dong, Chinese J. Struct. Chem. 27 (2008) 183; (c) L. Wang, J.C. Ma, W.K. Dong, L.C.

Zhu, Y. Zhang, Z. Anorg, Allg. Chem. 642 (2016) 834; (d) L. Xu, L.C. Zhu, J.C. Ma, Y. Zhang, J. Zhang, W.K. Dong, Z. Anorg, Allg. Chem. 641 (2015) 2520.

[9] A.G. Zavozin, N.I. Simirskaya, Y.V. Nelyubina, G.Z. Sergei, Tetrahedron 72 (2016) 7552.

[10] (a) L.Q. Chai, G. Liu, Y.L. Zhang, J.J. Huang, J.F. Tong, J. Coord. Chem. 66 (2013) 3926; (b) L.Q. Chai, G. Wang, Y.X. Sun, W.K. Dong, L. Zhao, X.H. Gao, J. Coord. Chem. 65 (2012) 1621; (c) L.Q. Chai, J.J. Huang, H.S. Zhang, Y.L. Zhang, J.Y. Zhang, Y.X. Li, Spectrochim. Acta Part A 131 (2014) 526; (d) L.Q. Chai, H.S. Zhang, J.J. Huang, Y.L. Zhang, Spectrochim. Acta Part A 137 (2015) 661.

[11] J. Olguin, M. Kalisz, R. Clerac, S. Brooker, Inorg. Chem. 51 (2012) 5058.

[12] Q. Mei, Q. Hua, B. Tong, Y.J. Shi, C. Chen, W. Huang, Tetrahedron 71 (2015) 9366.

[13] Ş. Ömer, Ö.Ö. Ümmühan, S. Nurgul, A. Burcu, S. Musa, T. Tuncay, S. Zeynel, Tetrahedron 72 (2016) 5843.

[14] (a) W.K. Dong, J.C. Ma, L.C. Zhu, Y. Zhang, New. J. Chem. 40 (2016) 6998; (b) W.K. Dong, J.C. Ma, Y.J. Dong, L.C. Zhu, Y. Zhang, Polyhedron 115 (2016) 228; (c) W.K. Dong, J.Y. Shi, J.K. Zhong, Y.Q. Tian, J.G. Duan, Chinese J. Inorg. Chem. 24 (2008) 10; (d) W.K. Dong, Y.X. Sun, X.N. He, J.F. Tong, J.C. Wu, Spectrochim. Acta, Part A 76 (2010) 476; (e) W.K. Dong, J.C. Ma, Y.X. Sun, S.F. Akogun, Y. Zhang, Cryst Growth Des. 16 (2016) 6903; (f) W.K. Dong, J.C. Ma, Y.J. Dong, Li. Zhao, L.C. Zhu, Y.X. Sun, Y. Zhang, J. Coord. Chem. 69 (2016) 3231; (g) W.K. Dong, J. Zhang, Y. Zhang, N. Li, Inorg. Chim. Acta 444 (2016) 95.

[15] (a) S. Akine, T. Taniguchi, T. Nabeshima, J. Am. Chem. Soc. 128 (2006) 15765; (b) T. Nabeshima, H. Miyazaki, A. Iwasaki, S. Akine, T. Saiki, C. Ikeda, Tetrahedron 63 (2007) 3328; (c) S. Akine, T. Tadokoro, T. Nabeshima, Inorg. Chem. 51 (2012) 11478; (d) T. Nabeshima, S. Akine, C. Ikeda, M. Yamamura, Chem. Lett. 39 (2010) 10; (e) S. Akine, T. Nabeshima, Dalton Trans. 47 (2009) 10395; (f) T. Nabeshima, D. Nishida, T. Saiki, Tetrahedron 59 (2003) 639.

[16] H.A. Tran, J. Collins, P.E. Georghiou, New J. Chem. 32 (2008) 1175.

[17] SMART & SAINT Software Reference Manuals, version 6.45; Bruker Analytical X-ray Systems, Inc.: Madison, WI, (2003).

[18] G.M. Sheldrick, Acta Crystallogr., Sect. A. A64 (2008) 112.

[19] R. Davila, N. Farias, E.C. Sanudo, A. Vega, A. Escuer, M. Soler, J. Manzur, New J. Chem. 40 (2016) 6164.

[20] T. Masaaki, N. Koshiro, F. Takeshi, M. Naohide, S. Yukinari, K. Masaaki, M. Naotaka, I. Takayuki, R. Nazzareno, M. Jerzy, Inorg. Chem. 52 (2013) 6160.

[21] A.W. Addison, T.N. Rao, J. Reedijk, V.J. Rijn, G.C. Verschoor, J. Am. Chem. Soc., Dalton Trans. (1984) 1349.

[22] C. Cannes, F. Bedioui, C. Gueugnot, J.Y. Nedelec, J. Devynck, New J. Chem. 23 (1999) 489.

[23] W.X. Feng, Y. Zhang, Z. Zhang, X.Q. Lu, H. Liu, G.X. Shi, D.J. Zou, D.D. Song, W. Fan, K. Wang, R.A. Jones, Inorg. Chem. 51 (2012) 11377.

[24] P.Y. Seth, A. Figuerola, J. Jover, E. Ruiz, A. Ghosh, Inorg. Chem. 53 (2014) 9296.

[25] R. Cyril, T. Jan, M. Jozef, E. George, O.F. Kostakis, M. Ruben, R. Boca, Polyhedron 126 (2017) 174.

[26] J. Vallejo, I. Castro, J. F. Soria, M. P. Deniz, C. Ruiz, F. Lloret, M. Julve, R. Ruiz, J. Cano, Inorg. Chem. 50 (2011) 2073.

[27] Y.H. Zhang, F. Yang, H. Hu, Q.L. Wang , G. M. Yang, D.Z. Liao, Inorg. Chem. Commun. 42 (2014) 33.

[28] C.J. Milios, A. Vinslava, A.G. Whittaker, S. Parsons, W. Wernsdorfer, G. Christou, S.P. Perlepes, E.K. Brechin, Inorg. Chem. 45 (2006) 5272.

[29] C. Rajnák, A. Packova, J. Titis, J. Miklovic, J. Moncol, R. Boca, Polyhedron 110 (2016) 85.

[30] J.A. Sheikh, A. Adhikary, H. S. Jena, S. Biswas, S. Konar, Inorg. Chem. 53 (2014) 1606.

[31] J. Vallejo, I. Castro, L.C. Delgado, C.R. Perez, J.F. Soria, R.R. Garcia, J. Cano, F. Lloret, M. Julve, Dalton Trans. 39 (2010) 2350.

[32] Z.H. Ni, L.F. Zhang, V. Tangoulis, W. Wernsdorfer, A.L. Cui, O. Sato, H.Z. Kou, Inorg. Chem. 46 (2007) 6029.

[33] F. Habib, I. Korobkova, M. Murugesu, Dalton Trans. 44 (2015) 6368.

[34] X.C. Huang, C. Zhou, D. Shao, X.Y. Wang, Inorg. Chem. 53 (2014) 12671.

[35] P. Antal, B. Drahos, R. Herchel, Z. Travnicek, Inorg. Chem. 55 (2016) 5957.

[36] F. Yang, Q. Zhou, Y.Q. Zhang, G. Zeng, G.H. Li, Z. Shi, B.W. Wang, S.H. Feng, Chem. Commun. 49 (2013) 5289.

Table 1

Crystallographic data and refinement parameters for complexes **1**-**4**.

Complex	**1**	**2**	**3**	**4**
Empirical formula	$C_{40}H_{44}Cl_6N_4O_{16}Co_3$	$C_{36}H_{34}CaN_4O_{14}Co_2$	$C_{36}H_{34}SrN_4O_{14}Co_2$	$C_{39.5}H_{44}BaN_4O_{16.5}Co_2$
Formula weight	1226.28	904.61	952.15	1093.98
T(K)	293(10)	297(10)	293(2)	294(2)
Radiation (Å)	Mo $K\alpha$, 0.71073	Mo $K\alpha$, 0.71073	Cu $K\alpha$, 1.54184	Mo $K\alpha$, 0.71073
Crystal system	monoclinic	triclinic	triclinic	triclinic
Space group	$P2_1/n$	$P\bar{1}$	$P\bar{1}$	$P\bar{1}$
a (Å)	14.1780(12)	12.5293(11)	12.5545(11)	10.2217(6)
b (Å)	16.6498(14)	13.1610(19)	13.2283(10)	13.551(8)
c (Å)	23.873(2)	15.0421(17)	15.0117(12)	16.9476(10)
α (°)	90	109.147(12)	109.370(7)	74.825(5)
β (°)	100.520(9)	103.296(9)	103.548(7)	79.515(5)
γ (°)	90	100.181(9)	99.312(7)	81.710(5）
Volume (Å^3)	5540.8(8)	2192.9(5)	2207.2	2216.1(2)
Z	4	2	2	2
D_c (g cm^{-3})	1.470	1.370	1.433	1.639
Absorption coefficient (mm^{-1})	1.241	0.937	7.929	1.694
θ range for data collection (°)	3.570 to 23.882	3.806 to 24.942	4.504 to 69.676	3.663 to 23.831
F (000)	2492.0	928.0	964.0	1102.0
$h/k/l$ (min, max)	-17,17/-20,14/-28,29	-15,15/-16,16/-18,18	-14,15/-15,11/-18,18	-13,13/-18,17/-21,22
Crystal size (mm)	0.24×0.27×0.33	0.31×0.33×0.34	0.24×0.25×0.32	0.14×0.15×0.21
Reflections collected	22010/10873 [R_{int}=0.086]	14193/8464 [R_{int} =0.054]	15730/8176 [R_{int}=0.058]	25177/12334 [R_{int}=0.052]
Independent reflection	10873	8464	8176	12334
Data/restraints/parameters	10873/6/634	8464/0/518	8176/0/518	12334/48/594
Final R indices [$I > 2\sigma(I)$][a]	R_1=0.0817	R_1= 0.0555	R_1= 0.0616	R_1=0.0569
	wR_2= 0.1916	wR_2= 0.1150	wR_2= 0.1678	wR_2= 0.1097
R indices (all data)[b]	R_1= 0.1357	R_1= 0.0901	R_1= 0.0791	R_1=0.1204
	wR_2= 0.2436	wR_2= 0.1366	wR_2= 0.1869	wR_2=0.1212
CCDC deposit number	1519396	1519397	1519394	1519395

a $R_1 = \Sigma||F_o| - |F_c||/\Sigma|F_o|$; *b*. $wR_2 = [\Sigma w(F_o^2 - F_c^2)^2/\Sigma w(F_o^2)^2]^{1/2}$, $w = [\sigma^2(F_o^2) + (0.0784P)^2 + 1.3233P]^{-1}$, where $P = (F_o^2 + 2F_c^2)/3$;

Table 2

Selected bond lengths (Å) and angles (°) of complexes **1**-**4**.

Complex **1**					
Co3-O5	2.071(4)	Co3-O6	2.030(3)	Co3-O12	2.027(3)
Co3-O14	2.040(4)	Co3-O15	2.150(4)	Co3-O(16)	2.141(4)
O5-Co3-O6	79.44(14)	O5-Co3-O12	97.60(14)	O5-Co3-O14	169.83(17)
O5-Co3-O15	83.38(17)	O5-Co3-O16	95.33(17)	O6-Co3-O12	172.22(16)
O6-Co3-O14	96.09(17)	O6-Co3-O15	87.94(18)	O6-Co3-O16	86.91(18)
O12-Co3-O14	87.95(18)	O12-Co3-O15	98.91(18)	O12-Co3-O16	86.20(18)
O14-Co3-O15	87.36(17)	O14-Co3-O16	93.53(18)	O15-Co3-O16	174.84(19)
Complex **2**					
Ca1-O1	2.604(3)	Ca1-O2	2.435(3)	Ca1-O5	2.384(3)
Ca1-O6	2.421(3)	Ca1-O9	2.395(3)	Ca1-O10	2.612(3)
Ca1-O12	2.405(4)	Ca1-O14	2.397(4)	O1-Ca1-O2	61.14(9)
O1-Ca1-O5	123.01(9)	O1-Ca1-O6	151.78(10)	O1-Ca1-O9	107.81(10)
O1-Ca1-O10	68.43(10)	O1-Ca1-O12	109.11(10)	O1-Ca1-O14	75.33(10)
O2-Ca1-O5	65.51(9)	O2-Ca1-O6	128.03(10)	O2-Ca1-O9	166.84(10)
O2-Ca1-O10	105.94(9)	O2-Ca1-O12	77.26(10)	O2-Ca1-O14	103.82(10)
O5-Ca1-O6	63.42(9)	O5-Ca1-O9	127.22(10)	O5-Ca1-O10	148.21(11)
O5-Ca1-O12	76.08(10)	O5-Ca1-O14	99.99(10)	O6-Ca1-O9	65.12(9)
O6-Ca1-O10	122.43(10)	O6-Ca1-O12	99.11(11)	O6-Ca1-O14	76.47(11)
O9-Ca1-O10	61.68(9)	O9-Ca1-O12	101.47(10)	O9-Ca1-O14	78.57(10)
O10-Ca1-O12	72.14(11)	O10-Ca1-O14	111.79(12)	O12-Ca1-O14	175.16(12)
Complex **3**					
Sr1-O1	2.650(4)	Sr1-O2	2.565(4)	Sr1-O5	2.521(4)
Sr1-O6	2.514(4)	Sr1-O9	2.543(4)	Sr1-O10	2.672(4)
Sr1-O12	2.562(5)	Sr1-O14	2.538(5)		
O1-Sr1-O2	59.56(13)	O1-Sr1-O5	121.34(13)	O1-Sr1-O6	151.82(13)
O1-Sr1-O9	114.92(13)	O1-Sr1-O10	75.06(14)	O1-Sr1-O12	103.28(14)
O1-Sr1-O14	77.73(14)	O2-Sr1-O5	63.97(13)	O2-Sr1-O6	123.12(13)
O2-Sr1-O9	173.82(13)	O2-Sr1-O10	114.66(13)	O2-Sr1-O12	73.86(13)
O2-Sr1-O14	104.74(15)	O5-Sr1-O6	61.22(13)	O5-Sr1-O9	122.09(13)
O5-Sr1-O10	146.97(15)	O5-Sr1-O12	74.22(14)	O5-Sr1-O14	103.09(15)
O6-Sr1-O9	63.03(13)	O6-Sr1-O10	119.14(13)	O6-Sr1-O12	104.11(14)
O6-Sr1-O14	74.62(15)	O9-Sr1-O10	59.80(13)	O9-Sr1-O12	105.95(13)
O9-Sr1-O14	75.71(15)	O10-Sr1-O12	74.02(15)	O10-Sr1-O14	108.69(16)
O12-Sr1-O14	177.29(16)				
Complex **4**					
Ba1-O1	2.935(5)	Ba1-O2	2.781(5)	Ba1-O5	2.751(5)
Ba1-O6	2.733(5)	Ba1-O9	2.851(5)	Ba1-O10	3.109(5)
Ba1-O12	2.789(7)	Ba1-O14	2.747(7)	Ba1-O16	2.797(15)
O1-Ba1-O2	54.73(14)	O1-Ba1-O5	103.83(13)	O1-Ba1-O6	124.63(14)
O1 -Ba1-O9	134.40(15)	O1-Ba1-O10	132.21(13)	O1-Ba1-O12	111.50(15)

O1-Ba1-O14	71.56(16)	O1-Ba1-O16	67.8(4)	O2-Ba1-O5	58.90(13)
O2-Ba1-O6	110.67(14)	O2-Ba1-O9	166.77(14)	O2-Ba1-O10	133.29(15)
O2-Ba1-O12	68.15(15)	O2-Ba1-O14	113.73(16)	O2-Ba1-O16	81.8(4)
O5-Ba1-O6	55.80(13)	O5-Ba1-O9	107.88(13)	O5-Ba1-O10	119.02(13)
O5-Ba1-O12	70.46(14)	O5-Ba1-O14	108.03(16)	O5-Ba1-O16	132.1(5)
O6-Ba1-O9	56.90(14)	O6-Ba1-O10	97.89(13)	O6-Ba1-O12	107.64(14)
O6-Ba1-O14	69.33(15)	O6-Ba1-O16	165.8(3)	O9-Ba1-O10	51.35(14)
O9-Ba1-O12	109.55(15)	O9-Ba1-O14	67.99(16)	O9-Ba1-O16	110.0(4)
O10-Ba1-O12	68.33(15)	O10-Ba1-O14	110.60(16)	O10-Ba1-O16	68.1(3)
O12-Ba1-O14	176.76(16)	O12-Ba1-O16	69.9(5)	O14-Ba1-O16	112.7(5)

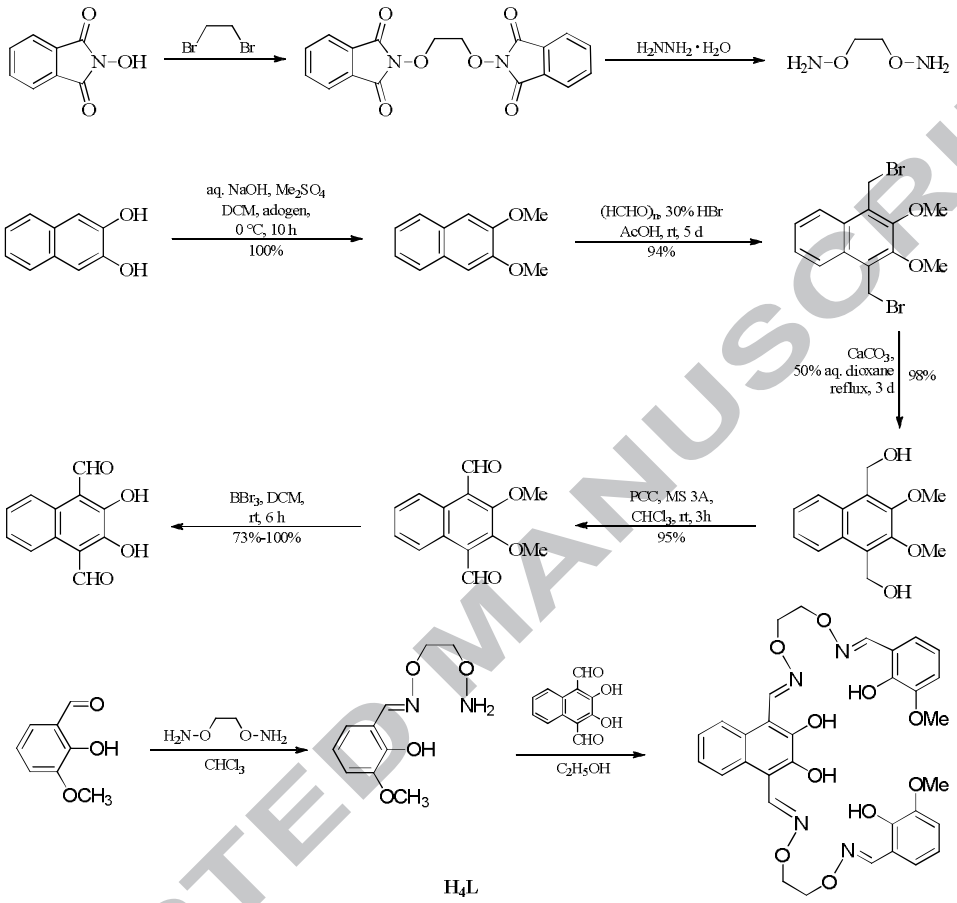

H_4L

Scheme 1.

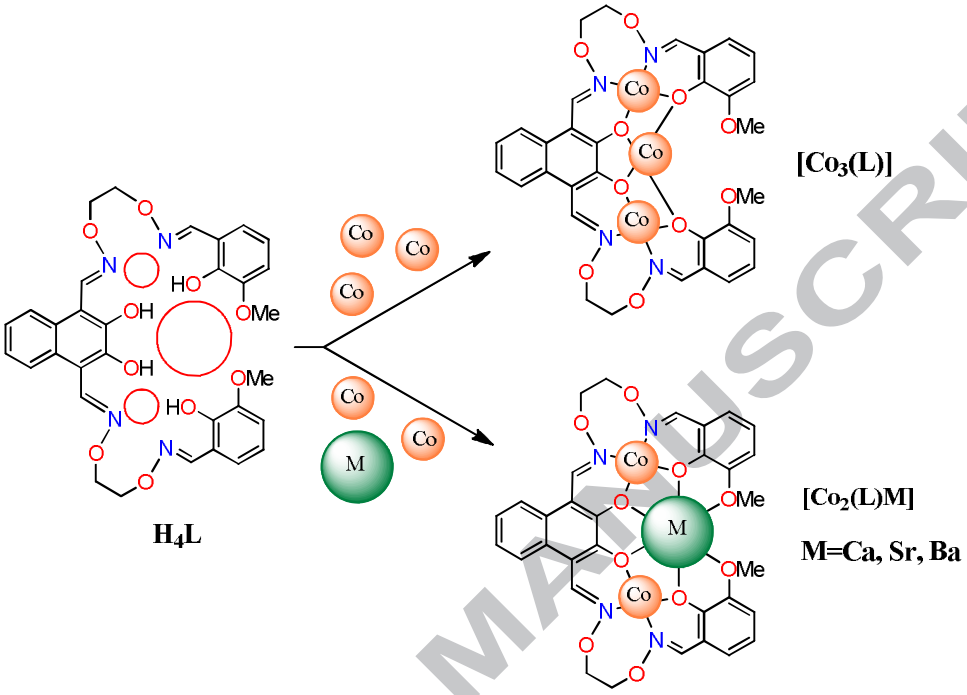

Scheme 2.

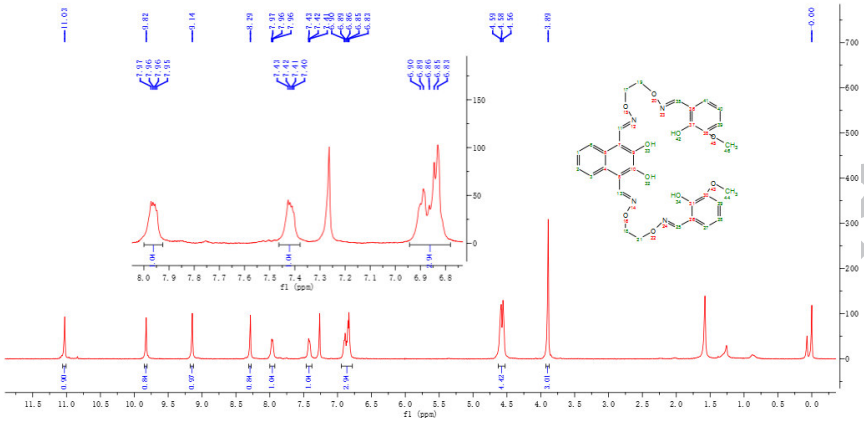

^{1}H NMR (400 MHz, $CDCl_3$) δ 11.03 (s, 2H), 9.82 (s, 2H), 9.14 (s, 2H), 8.29 (s, 2H), 7.97 (q, J = 3.2 Hz, 2H), 7.41 (q, J = 6.0, 2.9 Hz, 2H), 7.06 – 6.68 (m, 6H), 4.58 (t, 8H), 3.89 (s, 6H).

Fig. 1.

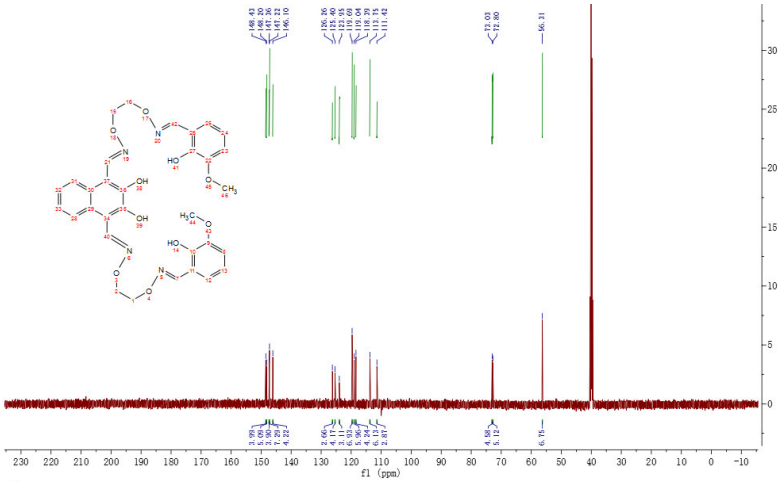

^{13}C NMR (151 MHz, DMSO) δ 148.43 (s), 148.20 (s), 147.36 (s), 147.22 (s), 146.10 (s), 126.26 (s), 125.40 (s), 123.95 (s), 119.69 (s), 119.04 (s), 118.39 (s), 113.75 (s), 111.42 (s), 73.03 (s), 72.80 (s), 56.31 (s).

Fig. 2.

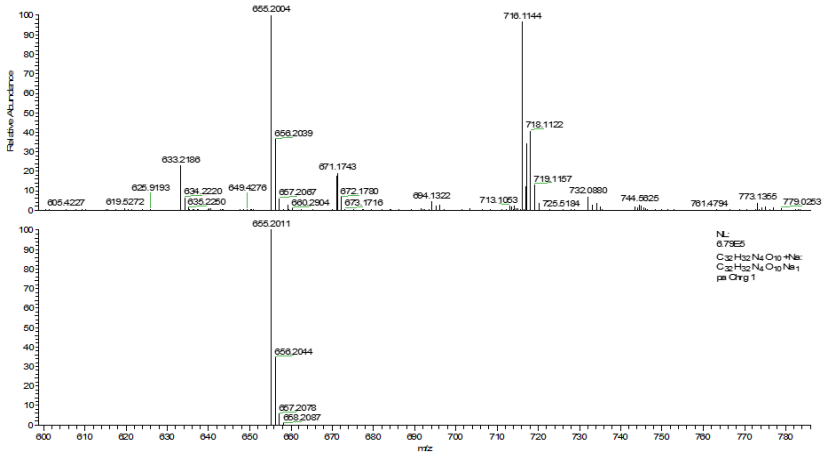

Fig. 3.

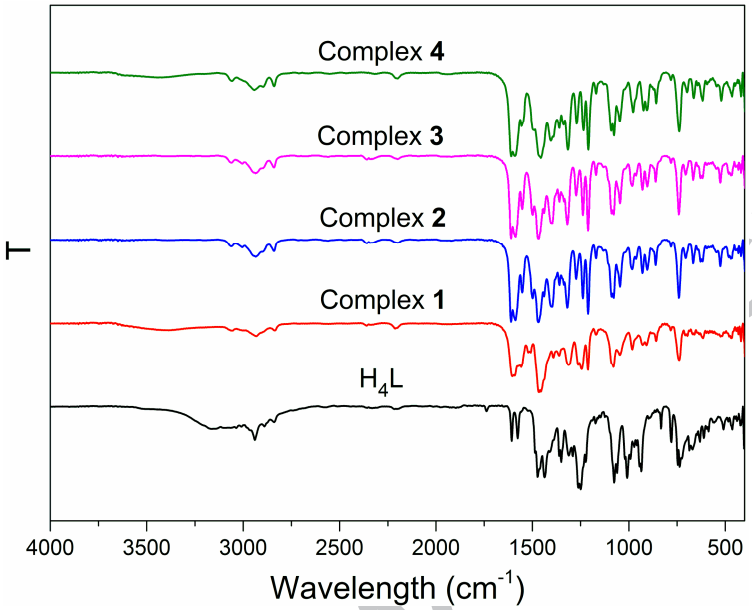

Fig. 4.

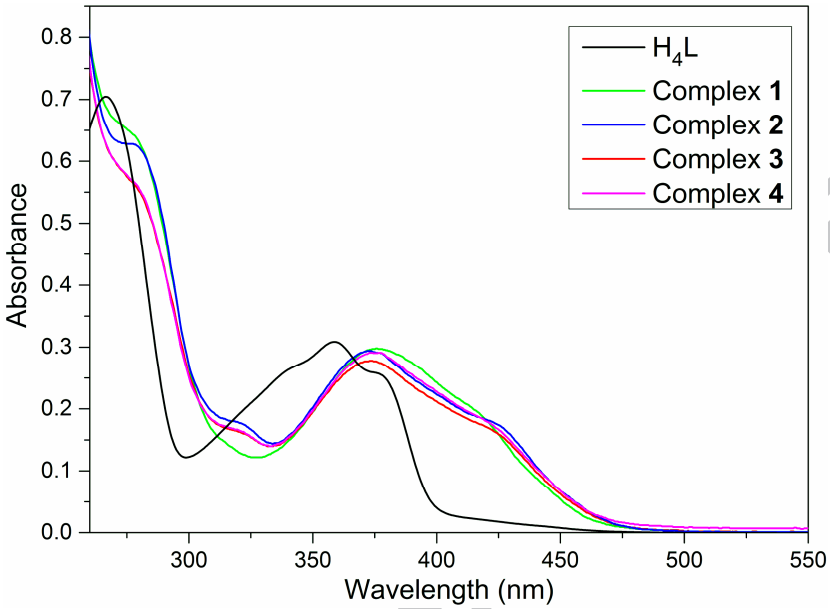

Fig. 5.

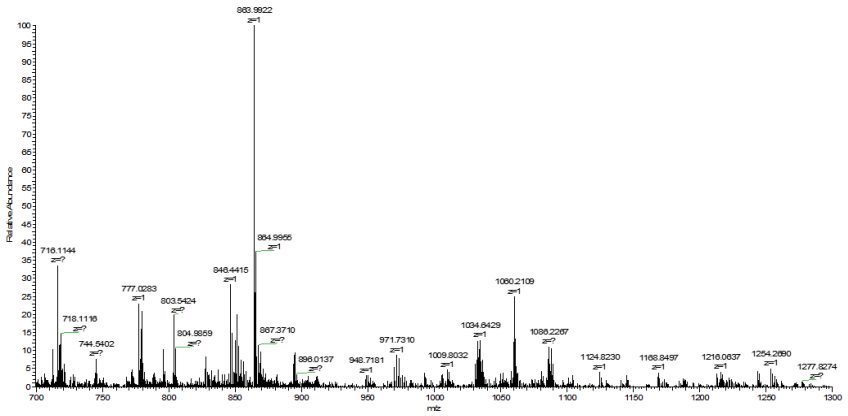

Fig. 6.

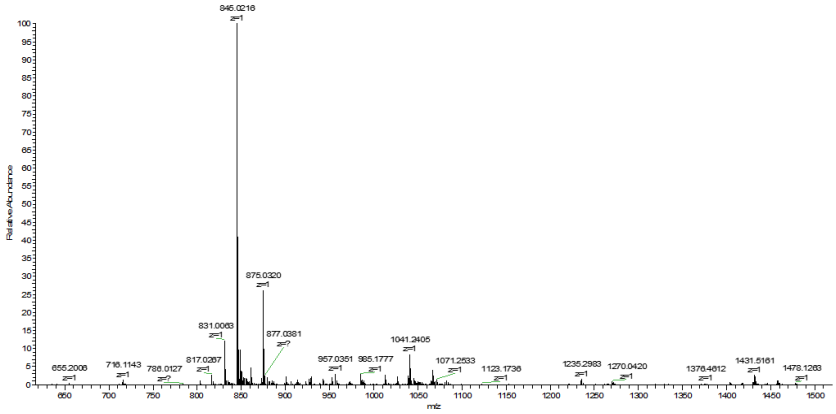

Fig. 7.

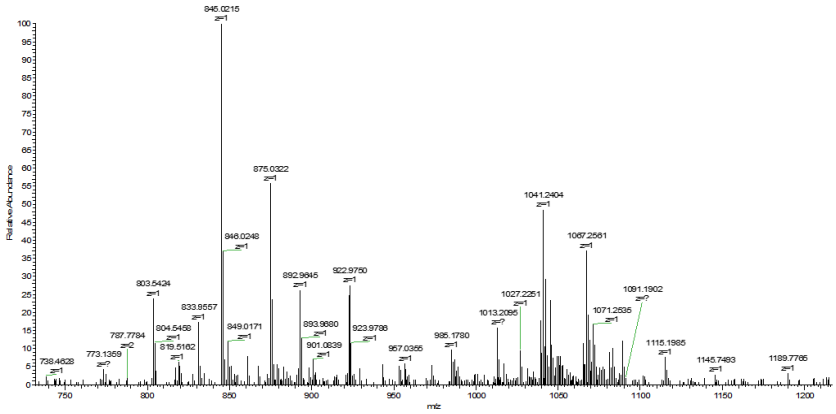

Fig. 8.

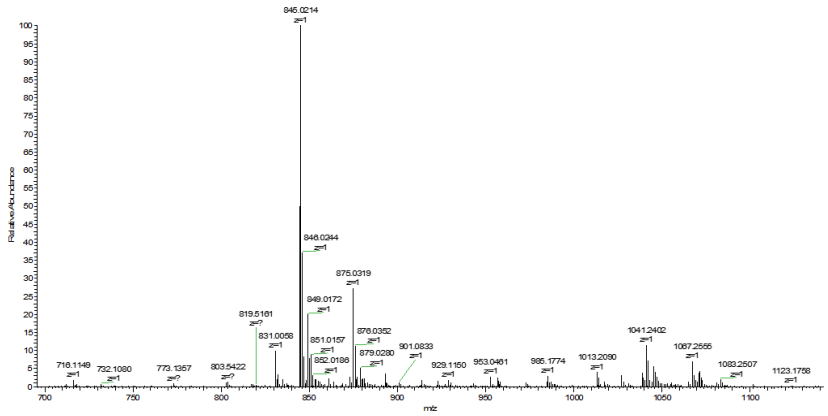

Fig. 9.

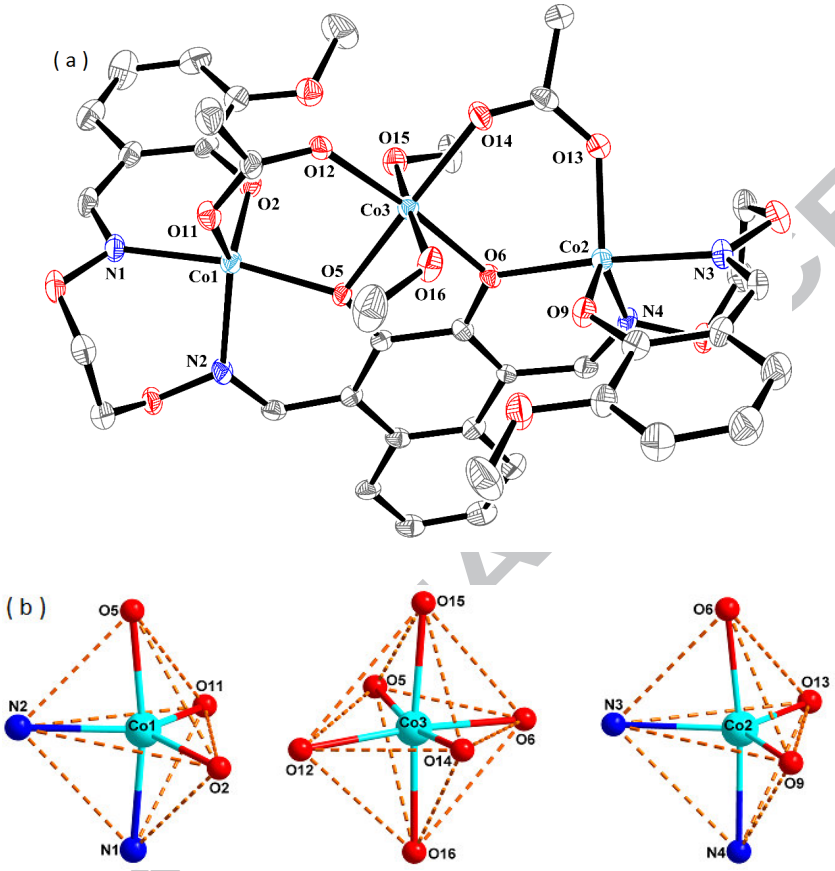

Fig. 10.

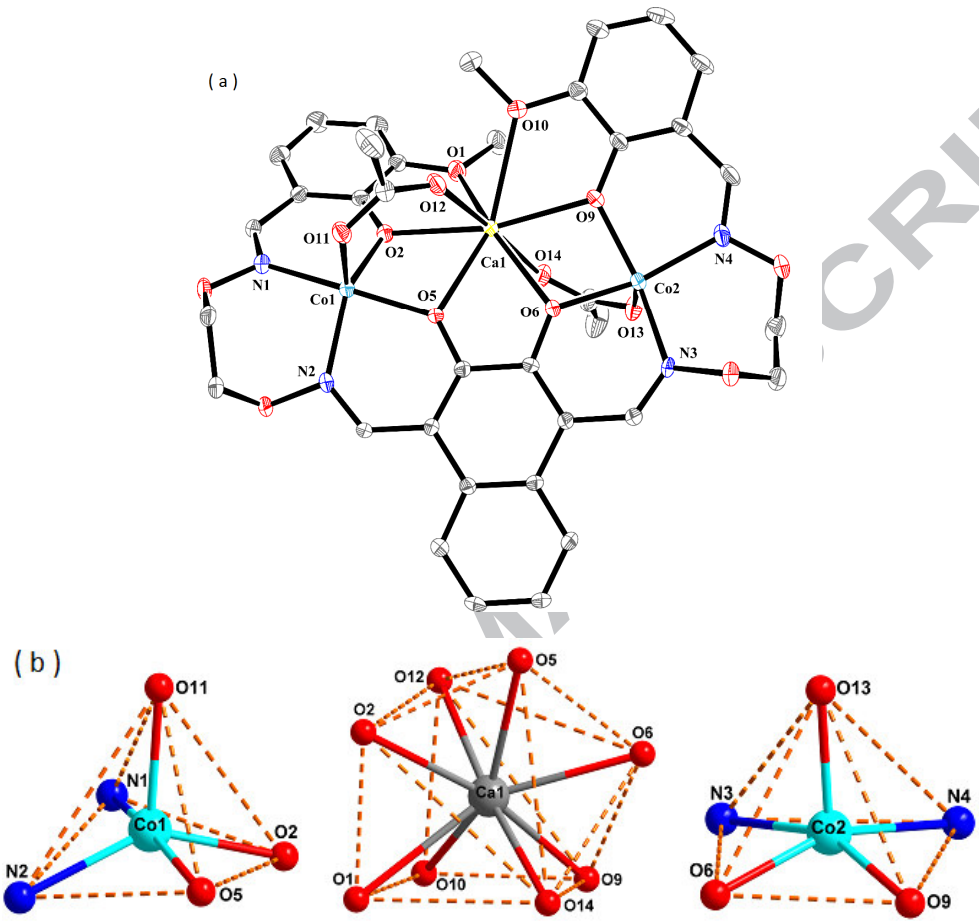

Fig. 11.

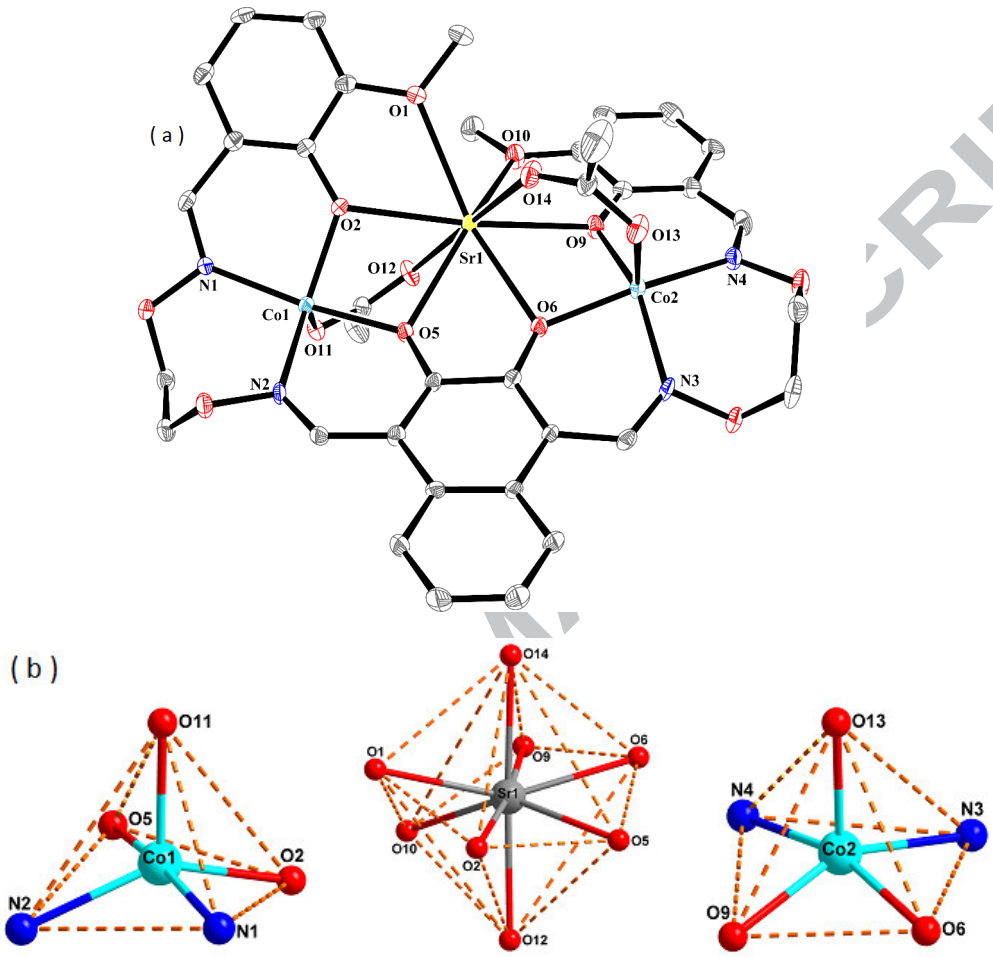

Fig. 12.

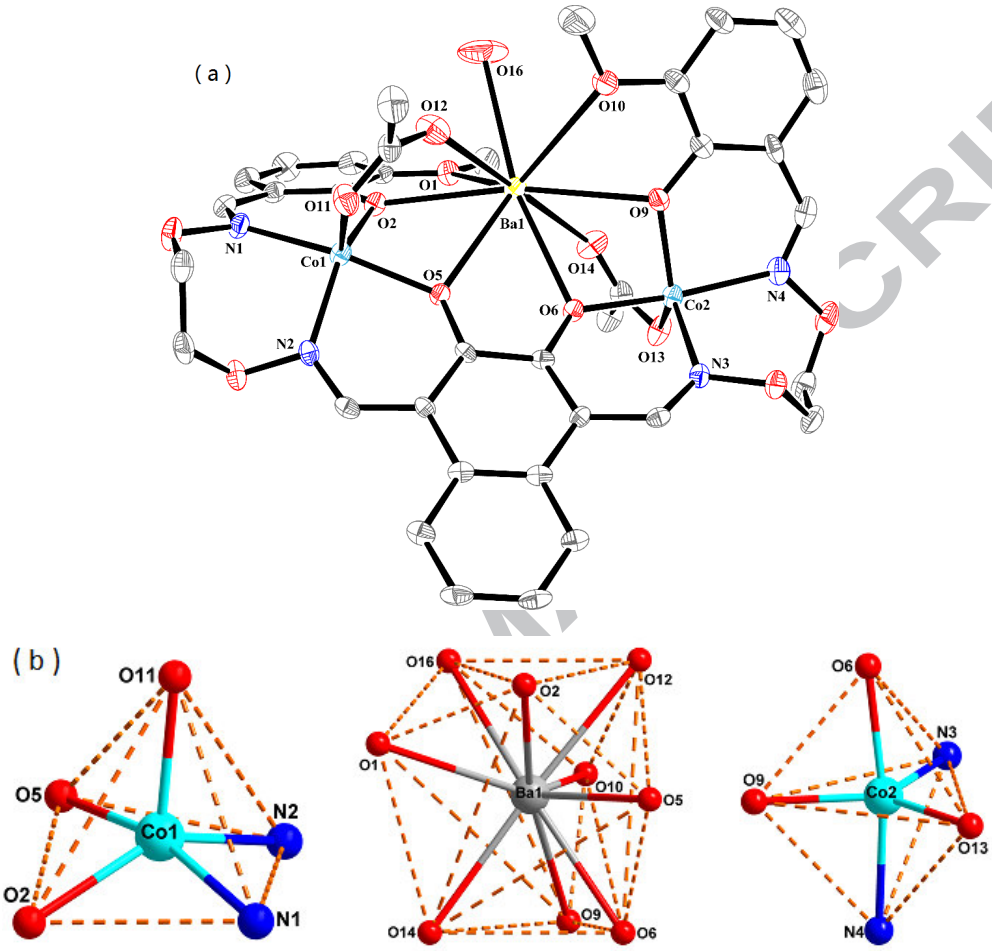

Fig. 13.

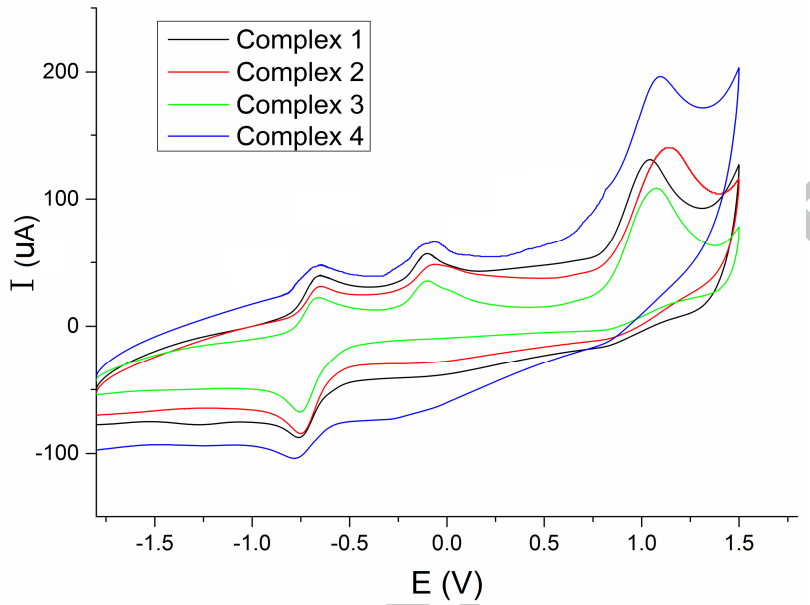

Fig. 14.

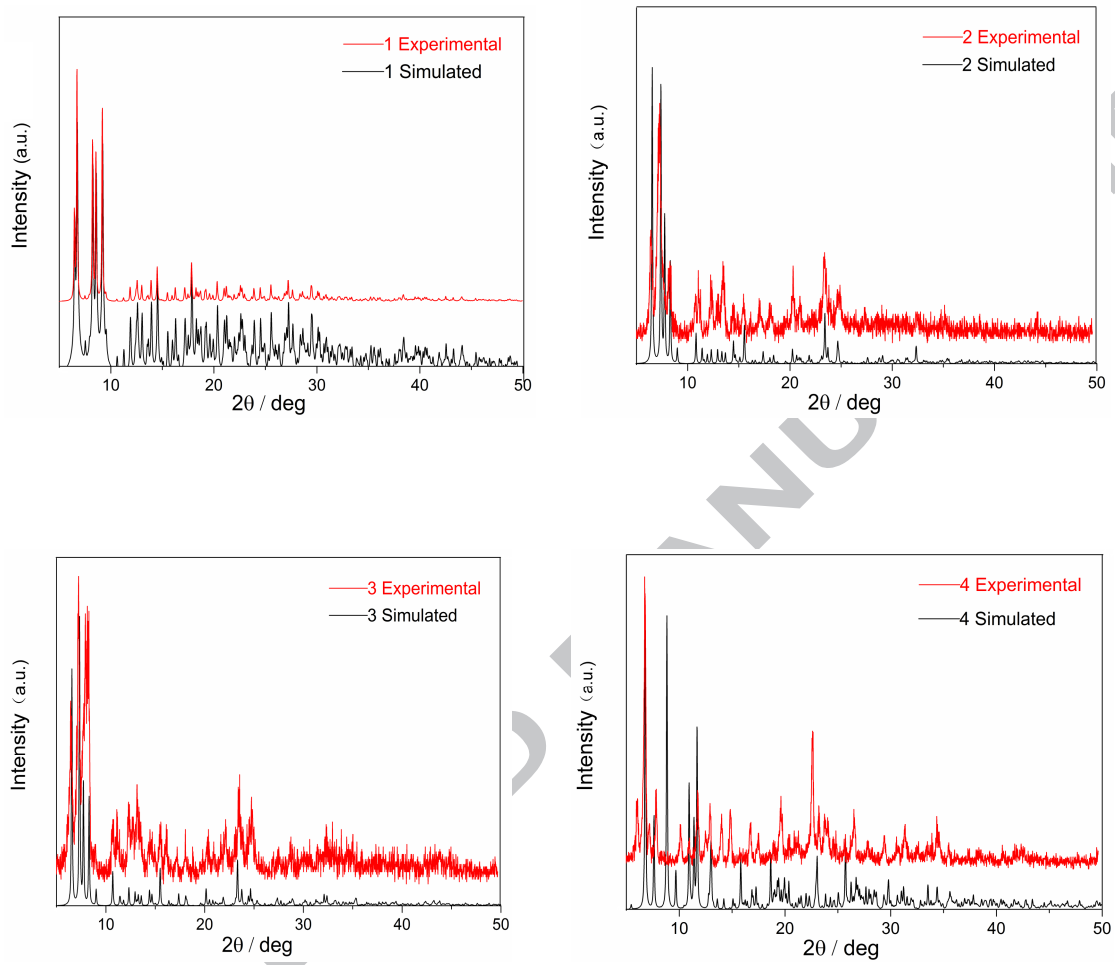

Fig. 15.

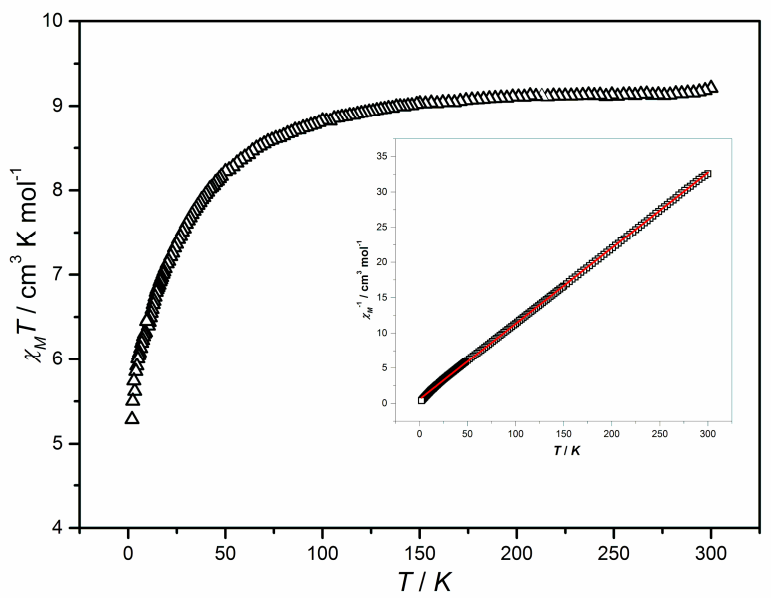

Fig. 16.

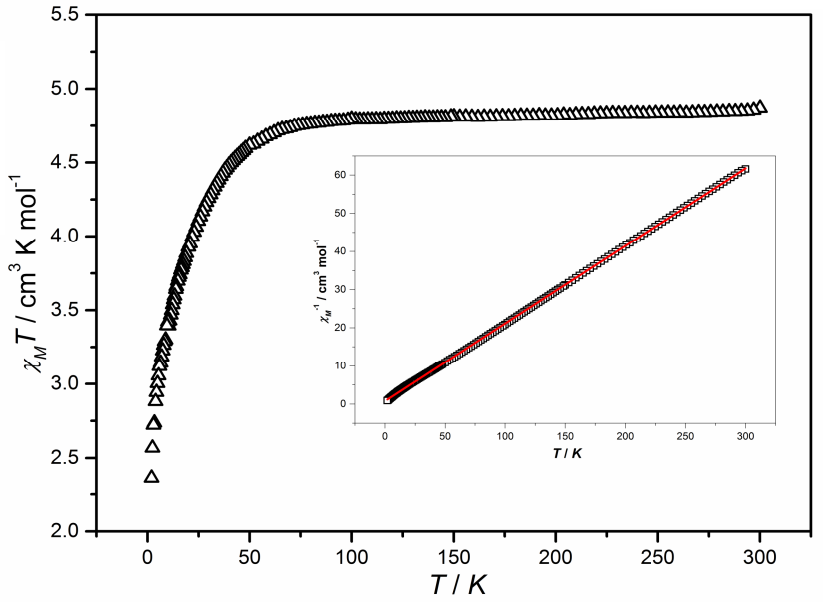

Fig. 17.

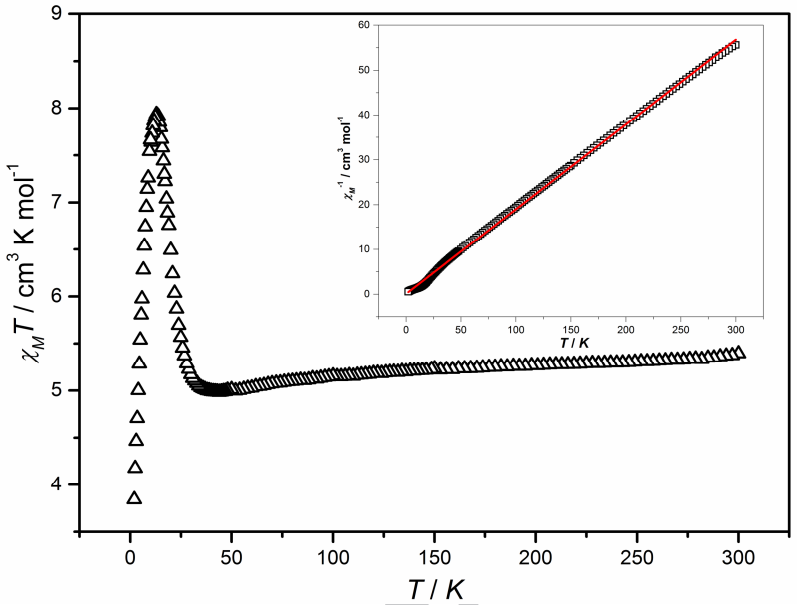

Fig. 18.

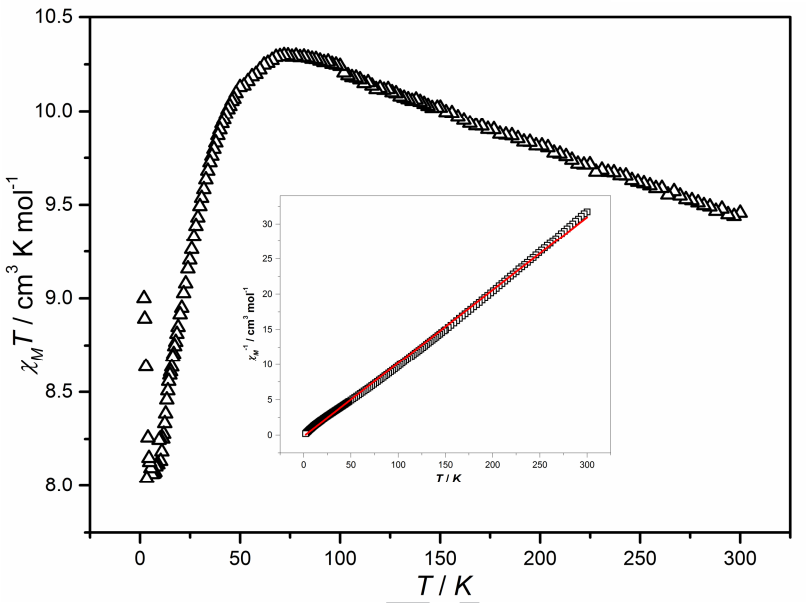

Fig. 19.

Graphical Abstract:

The homo- and heterotrinuclear Co(II) complexes $[Co_3(L)(OAc)_2(CH_3OH)_2]\cdot 2CHCl_3$ (**1**), $[Co_2(L)Ca(OAc)_2]$ (**2**), $[Co_2(L)Sr(OAc)_2]$ (**3**) and $[Co_2(L)Ba(OAc)_2(H_2O)]\cdot 2CH_3CH_2OH$ (**4**), constructed from the naphthalenediol-based acyclic bis(Salamo)-type ligand H_4L, show different crystal structures. Different intramolecular magnetic interactions are found in the homo/hetero-trinuclear complexes **1**-**4**.

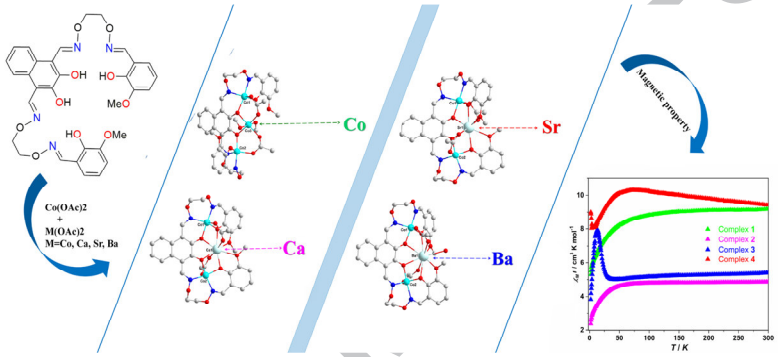

Graphical Abstract-pictogram